Published by IOP Publishing for Sissa Medialab

Received: *September 29, 2025*
Revised: *January 9, 2026*
Accepted: *January 14, 2026*
Published: *February 17, 2026*

26th International Workshop on Radiation Imaging Detectors
Bratislava, Slovakia
6–10 July 2025

# DQE analysis of CdTe and Si sensor Timepix3 detectors

**Pinelopi Christodoulou**[a,b,c,*] **Michael Campbell**,[a] **Tristan Genetay**[d,e] **Lukas Tlustos**[a,b] **and Jan Zemlicka**[b]

[a] *EP Department CERN, 1211 Geneva 23, Switzerland*
[b] *Institute of Experimental and Applied Physics, Czech Technical University of Prague, Husova 240/5, 110 000 Prague 1, Czech Republic*
[c] *Faculty of Biomedical Engineering, Czech Technical University in Prague, Nam Sitna 3105, 272 01 Kladno 2, Czech Republic*
[d] *HSE Department CERN, 1211 Geneva 23, Switzerland*
[e] *Institute of Radiation Physics, Lausanne University Hospital and Lausanne University, Lausanne, Switzerland*

*E-mail:* pinelopi.christodoulou@cern.ch

Abstract: In this study, the Detective Quantum Efficiency (DQE) was measured by calculating the DQE at zero-frequency, the modulation transfer function (MTF), and the noise power spectrum (NPS) for Timepix3 detectors (pixel size of 55 µm) equipped with 500 µm silicon (Si) sensor and 1mm Cadmium Telluride (CdTe) sensor, with a Tungsten X-ray tube of 40 kVp (narrow-spectrum series (N-series) with beam quality N-40). By comparing these parameters, the impact of sensor material on spatial resolution and noise characteristics was assessed. In this study the MTF, NPS and DQE parameters were calculated with datasets from two different acquisition modes; counting mode, where the particle hits are not clustered and Time of Arrival and Time over Threshold (energy) mode, where the particle hits are clustered and their center of mass (c.m.) is calculated. It was concluded that the c.m. dataset provided better MTF and NPS values leading to an improved DQE estimation. It was also possible to correct the charge sharing caused by fluorescence events in the CdTe sensor by identifying the clusters, reconstructing the energy of the initial particle and assigning this energy to the position of the initial hit that generated the fluorescent photon. It was shown that the CdTe sensor offers an overall better detector performance than the Si sensor for high-resolution imaging applications for the chosen energy range. Systems with higher DQE can produce images with better contrast and lower noise, making them ideal for dose-sensitive applications like medical imaging.

Keywords: Hybrid detectors; Interaction of radiation with matter; Solid state detectors

*Corresponding author.



https://doi.org/10.1088/1748-0221/21/02/C02024

## Contents


**1 Introduction** **1**

**2 Methodology** **2**

2.1 Detective Quantum Efficiency 2

**3 Results** **4**

**4 Discussion and conclusion** **6**




## 1 Introduction

The Detective Quantum Efficiency (DQE) is a fundamental metric for assessing the imaging performance of X-ray detectors. It quantifies how effectively a detector transfers the signal-to-noise ratio (SNR) from the incident X-ray beam to the final image, accounting for noise sources, signal transfer characteristics, and spatial resolution. A high DQE indicates that the detector preserves image quality while minimizing noise, which is critical for achieving diagnostic accuracy or precise material characterization at the lowest possible radiation dose. This makes DQE optimization a central goal in medical imaging, industrial inspection, and scientific applications. Photon Counting Detectors (PCDs) have emerged as a transformative technology in X-ray imaging, offering advantages such as energy discrimination, reduced electronic noise, and improved dose efficiency compared to conventional integrating detectors. These detectors, exemplified by the Medipix family developed by the Medipix Collaboration [1], enable spectral imaging and quantitative material decomposition, which are increasingly important in advanced diagnostic and research settings. However, the performance of PCDs is strongly influenced by physical and technological factors, including detector material (e.g., CdTe, Si, GaAs) [2], energy resolution [3], pixel size [4], and readout electronics [5]. Each of these parameters affects the modulation transfer function (MTF), noise power spectrum (NPS), and ultimately the DQE. Recent research has focused on mitigating limitations inherent to PCDs, such as charge sharing between pixels, pulse pile-up at high flux, and fluorescence escape in high-Z materials. For instance, Monte Carlo simulations have demonstrated that coincidence-based charge-sharing correction can significantly improve spatial resolution and DQE [6]. Similarly, advanced clustering algorithms leveraging time-over-threshold (ToT) and time-of-arrival (ToA) information have been proposed to enhance energy weighting and reduce noise artifacts. These developments align with broader trends in detector technology, where computational methods and hardware innovations are combined to push the boundaries of resolution, efficiency, and spectral fidelity. In this work, we present a comparative study of Si and CdTe-based PCDs, focusing on their imaging performance as characterized by DQE, MTF, and normalized NPS (NNPS) for Timepix3 detectors [7]. We investigate the impact of energy-weighted center-of-mass clustering using ToT and ToA data, as well as the influence of fluorescence events in CdTe detectors. Our results provide new insights into the interplay between detector physics and image quality, and propose strategies for optimizing PCD performance in high-precision X-ray imaging applications, such as medical diagnostics, synchrotron experiments, and non-destructive testing.

## 2 Methodology

### 2.1 Detective Quantum Efficiency

The DQE can be calculated using equation (2.1), where DQE(0) represents the DQE at zero spatial frequency, MTF is the Modulation Transfer Function and NNPS is the Normalized Noise Power Spectrum.

$$\mathrm{DQE}(f) = \mathrm{DQE}(0) \cdot \frac{\mathrm{MTF}(f)^2}{\mathrm{NNPS}(f)} \tag{2.1}$$

#### 2.1.1 DQE(0)

In PCDs phenomena such as charge sharing can cause a single photon to be counted in multiple pixels, impacting the DQE as described in [8]. DQE at zero frequency can be calculated with equation (2.2), where $\epsilon$ is the detection efficiency and $m$ is the multiplicity.

$$\mathrm{DQE}(0) = \epsilon \cdot \frac{\langle m \rangle^2}{\langle m^2 \rangle} \tag{2.2}$$

To obtain the correct value for $\epsilon$ ($\epsilon = \frac{Ntrue}{Nin}$) it is necessary to accurately measure the number of photons that arrive on the detector ($Nin$) and compare them to the number of photons that are measured by the detector ($Ntrue$). For that purpose a calibrated ionization chamber PTW 23361 (PTW, Freiburg, Germany) was placed in front of the X-ray tube (X80-320 X-ray beam irradiator, Hopewell designs, Alpharetta, U.S.A.) in the dosimetry laboratory of the European Organization for Nuclear Research (CERN) facility in Geneva. More specifically, the narrow-spectrum series (N-series) with beam quality N-40 was chosen. The tube's anode is made of tungsten (W), the operating voltage is set to 40 kV and the current to 0.5 mA. The N-40 series has a built-in filter of 4 mm Al with an additional 0.21 mm of Cu. This provides an incoming spectrum reaching up to 40 keV with a mean energy of around 33 keV.

The ionization chamber was placed 2.5 m away from the X-ray irradiator (i.e. the reference point from the device) and irradiated for 30 seconds. The ionization chamber, as the name suggests, can measure the amount of ionization produced by X-ray photons in a given volume of air. The amount of ionization is proportional to the energy deposited by the X-ray photons. The chamber was calibrated in a Secondary Standard Dosimetry Laboratory (SSDL) (PTW Calibration lab, Freiburg, Germany). The electrometer (PTW Unidos T10021) measured the charge deposited (Q) in the sensitive volume of the ionization chamber in Coulomb (C). This charge was then corrected by taking into account multiple parameters as mentioned in ISO 4037-1:2019[1] following the equation (2.3).

$$Q_{\mathrm{corrected}} = Q_{\mathrm{measured}} \cdot K_{T,P} \tag{2.3}$$

$K_{T,P}$ is a conversion factor that takes into account the variation caused by the temperature and the pressure and is calculated according to equation (2.4), where $P_0$ and $T_0$ are the reference values for the pressure and temperature given by the calibration certificate of the ionization chamber.

$$K_{T,P} = \frac{P_0 T}{T_0 P} \tag{2.4}$$

[1] https://www.iso.org/standard/66872.html.



2026 JINST 21 C02024

It is possible to convert the corrected charge to $K_{\text{air}}$ following equation (2.5).

$$K_{\text{air}} = N_K \cdot k_{Q,Q_0} \cdot Q_{\text{corrected}} \tag{2.5}$$

where $K_{\text{air}}$ is the air kerma, $N_K$ is the chamber conversion factor to kerma and $k_{Q,Q_0}$ is the beam quality factor. $K_{\text{air}}$ refers to the kinetic energy released per unit mass of air due to the interaction of ionizing radiation (such as X-rays) with the air. It is commonly measured in units of Gray (Gy).

Since the N-series has been calibrated with respect to ISO 4037, the spectral distribution is therefore considered as 'known' at the reference points. Then it is possible to use the kerma factors (in $pGy.cm^2$) provided by Ankerhold [9] to determine the particle fluence from the measurement of the ionization chamber. To verify that the fluence was measured correctly, the SpekPy library was used [10].

For the average cluster multiplicity equation (2.6) was considered for very short acquisition times, such that the average distance between the detected events is relatively large compared to the size of the pixel.

$$\langle m \rangle = \frac{N_{\text{meas}}}{N_{\text{true}}} \tag{2.6}$$

### 2.1.2 Modulation Transfer Function

The Modulation Transfer Function (MTF) is a critical parameter for assessing the performance of optical imaging systems, as it quantifies the system's ability to reproduce (or transfer) various levels of detail from the object to the image. One common method for measuring MTF is the knife-edge technique [11], also known as the slanted-edge method, which was followed in this study.

The first step is to acquire two sets of measurements. One set includes a radiographic image of an object with a sharp edge. The second set of measurements include acquisition of just the open beam, which is necessary for the flat field correction, in order to remove fixed pattern noise of the acquired image. A sample which includes a sharp edge of tungsten was placed directly in front of the detector with a small angle (2 degrees) so as to oversample the pixels and then irradiated with the X-ray source. Thanks to this technique, it is possible to detect the Edge Spread Function (ESF) by resampling on the axis perpendicular to the edge. The ESF is then fitted with an error function. The MTF can be calculated then by taking the magnitude of the Fourier Transform of the gradient of the fitted ESF.

It is important to ensure that the MTF is normalized to 1 in the low-frequency limit because at f=0 the spatial frequency corresponds to uniform (DC) signals, where there is no variation in intensity across the image. A perfect imaging system would transfer this uniform input signal fully. So by normalizing the MTF it becomes possible to make sure that the system's response is referenced to its maximum signal transfer capability and of course it is possible to directly compare the MTFs of different systems.

### 2.1.3 Noise Power Spectrum

The Noise Power Spectrum (NPS) quantifies the spatial distribution of noise in an image and is a crucial intermediate step in determining the Detective Quantum Efficiency (DQE) of photon-counting detectors (PCDs). The NPS is typically calculated by first acquiring flat-field images under uniform X-ray illumination and subtracting the mean signal to isolate noise fluctuations in each image. The two-dimensional Fourier transform of these noise-only images is computed, and the NPS is obtained by averaging the squared magnitude of the Fourier components over multiple flat-field subtracted noise images. To account for the pixel area, the NPS is normalized by the squared pixel size. The NPS were normalized to NPS(0) in order to be used in the equation (2.1) as NNPS.

## 3 Results

Following the methodology described in section 2.1.1 the noise amplification factor $\frac{\langle m \rangle^2}{\langle m^2 \rangle}$ for the measurements in the counting mode was calculated to be equal to 0.72 for CdTe and 0.57 for Si, while the efficiency $\epsilon$ is equal to 0.89 for CdTe and 0.11 for Si. By inserting the calculated values into equation (2.2) the $DQE(0)$ is calculated.

The MTF was calculated for the two Timepix3 detectors under the same conditions (beam energy and system alignment) therefore the results reflect the intrinsic detector performance. The Timepix3 assembly with the Si sensor was biased to 200 V and the threshold was set to 3 keV, while the bias for the assembly with the CdTe sensor was -300 V and the threshold was set to 5 keV. Two different sets of data were derived and used for each detector type; one set emulated the counting mode of the detectors in which the number of hits per pixel are simply added up while the other set used the Time of Arrival ($ToA$) and Time over Threshold ($ToT$) mode (*ToA & ToT*) and the hit data was clustered. For each cluster the center of mass (c.m.) was calculated, using the calibrated energy of the pixels as weights. In this clustered representation, each cluster was treated as a single event, characterized by its total energy and the position of its c.m., which was rounded to pixel values.

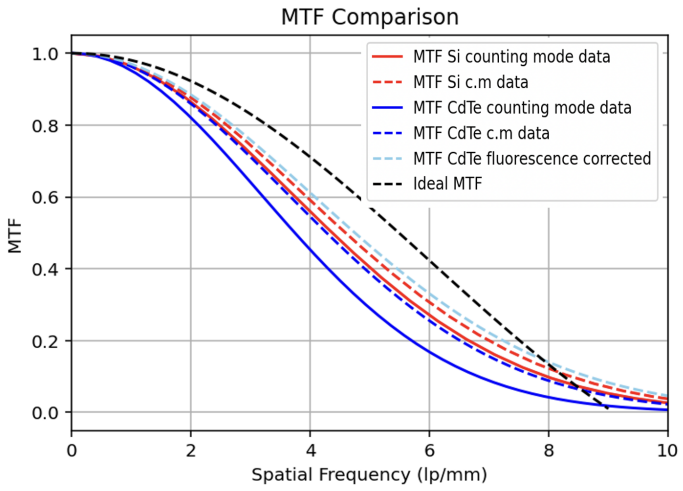


**Figure 1.** Comparison of the MTF for Si and CdTe sensors before and after the center-of-mass (c.m.) calculation and fluorescence correction in CdTe. The black dashed line shows the ideal MTF given by a sinc function. Solid lines correspond to counting mode without clustering, while dashed lines correspond to c.m. clustering using calibrated energy weighting.

The comparison of the MTFs is shown in figure 1, where the solid lines show the MTF for the unclustered data in counting mode while the dashed lines show the MTF for the c.m. data in the (*ToA & ToT*) mode. It can be noted that for the unclustered data, the MTF of the Si (red solid line) is better than the MTF of the CdTe (blue solid line). This can be explained by the increased charge sharing that occurs in the CdTe sensor which deteriorates the spatial resolution. CdTe sensors often exhibit more charge sharing due to their high-Z material and thicker detector layers. Si sensors on the other hand exhibit lower charge sharing, so they may maintain sharper signal localization, resulting in a higher MTF. However, by calculating the c.m. of the hits the MTF for the CdTe sensor (blue dashed lines) improves and almost reaches the MTF for the c.m. of the Si sensor (red dashed line).

This difference between the MTFs of the two sensors is due to fluorescence phenomenon which is more evident in the CdTe. For the studied energy range with the X-ray tube set to 40 kVp, the generation of fluorescent photons is more prominent for CdTe since Cd has a $K_\alpha$ = 23.2 keV as well as $K_\beta$ = 26.1 keV and Te has a $K_\alpha$ = 27.5 keV and $K_\beta$ = 31 keV, while Si has fluorescent photons below the threshold value of the detector ($K_\alpha$ = 1.74 keV). This generation of fluorescence affects negatively the spatial resolution of the CdTe sensors.

However, it is possible to correct for the fluorescence events of the CdTe sensor by taking advantage of the fact that with Timepix3 one has access to not only the spatial coordinates of the individual particle hits on the sensor but also their energy and time of arrival. Thanks to this feature, the fluorescent events in CdTe were not only located but also corrected by reassigning the total energy to the initial hit that generated the fluorescence event. More specifically, the dataset was filtered for events that could match the fluorescence energies of Cd and Te within a time window of 40 ns. The mean free path of these fluorescent particles were also taken into consideration to check the distance between the clusters. The result of the improvement of the MTF for the CdTe sensor can be seen in figure 1 where the MTF of the CdTe dataset with reassembled energies to correct for the fluorescent phenomena is plotted (dashed light blue line). The sub-threshold losses due to the phenomenon of charge sharing caused by the thermal diffusion and repulsion of the charge within the sensor, as shown in [12], is now the only effect that prevents the sensor from reaching the ideal behavior, as shown with the dashed black line in figure 1.

In figure 2 the comparison of the NNPS for the two different types of acquisition analysis (unclustered hits from the counting mode and c.m. hits from *ToA* & *ToT* data driven mode) are shown. All of the NNPS are calculated after flat fielding to avoid extra noise due to structures such as the contact pads for the high voltage in the CdTe and faulty pixels. The CdTe (blue solid and dashed line) displays a more noisy behavior regardless of whether the data is clustered or not. This could be attributed to the increased trapping and polarization effects in CdTe. As can be observed from figure 2, both Si and CdTe NNPS that were calculated using the c.m. data are flat at different spatial frequencies with Si offering a less noisy behavior.

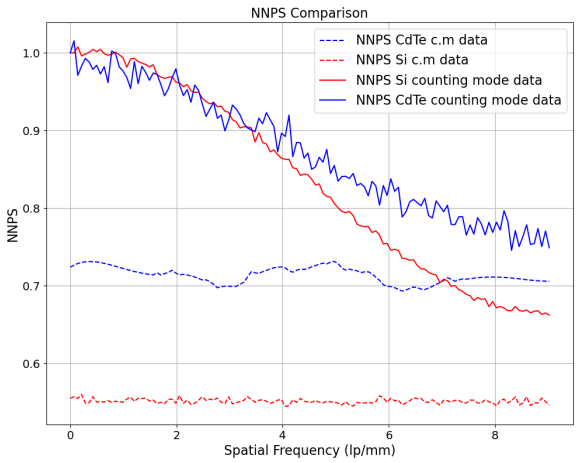


**Figure 2.** Comparison of the NNPS for Si and CdTe sensors using c.m. data. Solid lines correspond to counting-mode data, while dashed lines correspond to c.m.-clustered data using ToA and ToT information.



2026 JINST 21 C02024

By combining all the aforementioned components (DQE(0), MTF, NNPS) of the equation (2.1), it is now possible to calculate DQE and compare the results for the Si and CdTe sensors. The results are shown in figure 3.

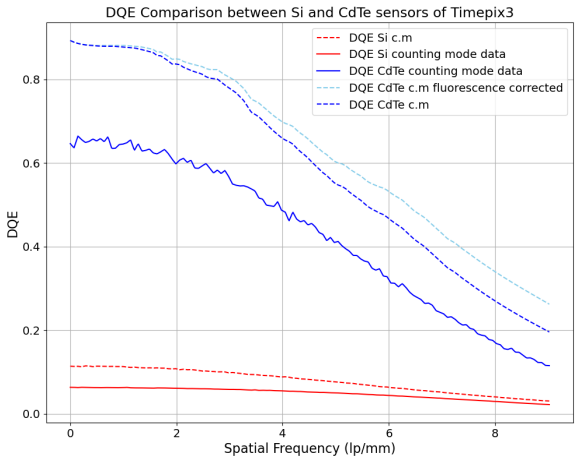


**Figure 3.** Comparison of the DQE for Si and CdTe sensors using MTF and NNPS from unclustered counting-mode data and clustered center-of-mass (c.m.) data from the data-driven mode. Dashed lines correspond to clustered (c.m) data-driven mode data, while solid lines correspond to unclustered data from the counting-mode.

It is clear that the calculation of c.m. improves the DQE for both sensor types (dashed lines) compared to the unclustered data (solid lines). For the low frequencies the CdTe sensor (blue line) has a much higher DQE(0) compared to the Si sensor (red line). The difference between the two CdTe DQE curves is the correction of the fluorescence events (light blue dashed line), which provides an improved DQE behavior compared to the uncorrected CdTe data (blue line). The fact that both CdTe DQE curves are higher than the Si DQE is expected because CdTe has a higher quantum efficiency due to its greater X-ray absorption. For the Si sensor the DQE starts at a much lower DQE(0), which is reasonable since silicon has lower stopping power for high-energy X-rays compared to CdTe.

For the middle range frequencies the CdTe DQE drops rapidly, which suggests that charge-sharing effects, carrier trapping, or incomplete charge collection impact its performance at higher spatial frequencies. The Si sensor maintains a more gradual decline, likely due to its better charge transport properties (lower charge sharing, less carrier trapping).

## 4 Discussion and conclusion

The DQE can be calculated for the specific spectrum provided by the N-40 series X-source, using the system's Modulation Transfer Function (MTF) and Noise Power Spectrum (NPS), two fundamental metrics that describe an imaging system's spatial resolution and noise characteristics, respectively. In this study it is shown that it is possible to improve the DQE of the Timepix3 detectors by simply calculating the c.m. by exploiting the information from the *ToA* & *ToT* data driven mode. In addition, in the case of the CdTe sensor, it is feasible to locate the fluorescence events and reassign the initial energy to the initial hit that generated them, which leads to further improvement of the DQE.



2026 JINST 21 C02024

Regarding the MTF, the c.m. calculation lead to the reduction of the charge sharing effectively improving the spatial resolution of the systems, which in turn improves the MTF. Even though the modulation transfer function (MTF) of the CdTe sensor is degraded due to the presence of fluorescence-induced charge sharing, the data-driven architecture of the Timepix3 detector, which records energy, time, and interaction coordinates for each detected event, enables a solution to this issue. By identifying fluorescence events and reassembling their energies based on spatial and temporal correlations, it is possible to mitigate their impact on spatial resolution.

Regarding the NNPS, in the unclustered data every triggered pixel is treated separately, leading to high-frequency noise, since there is an impact of correlated hits from multi pixel events. However, the c.m. clustering leads to uncorrelated white noise, which results in lower and constant NNPS.

Finally, by combining the improved MTF and NNPS it is possible to calculate the DQE of both sensor types for the same spectrum of X-ray source. The results of this study demonstrate that the DQE is higher for the CdTe Timepix3 detector compared to its Si counterpart, highlighting the superior quantum efficiency of CdTe in the studied energy range. The DQE of CdTe becomes even better after the reconstruction of the fluorescent events by taking advantage of the *ToA* & *ToT* information of the clusters in the data driven mode.

## Acknowledgments

The authors acknowledge funding from the CERN Medical Applications in the Knowledge Transfer Group and the Medipix3 collaboration.

## References

[1] R. Ballabriga, M. Campbell and X. Llopart, *An introduction to the Medipix family ASICs*, *Radiat. Meas.* **136** (2020) 106271.

[2] J. Scholz et al., *Biomedical x-ray imaging with a GaAs photon-counting detector: A comparative study*, *APL Photonics* **5** (2020) 106108.

[3] M. Persson, P.L. Rajbhandary and N.J. Pelc, *A framework for performance characterization of energy-resolving photon-counting detectors*, *Med. Phys.* **45** (2018) 4897 [arXiv:1803.07483].

[4] M. Persson, A. Wang and N.J. Pelc, *Detective quantum efficiency of photon-counting CdTe and Si detectors for computed tomography: a simulation study*, *J. Med. Imag.* **7** (2020) 043501.

[5] X. Ji, R. Zhang, G.-H. Chen and K. Li, *Impact of anti-charge sharing on the zero-frequency detective quantum efficiency of CdTe-based photon counting detector system: cascaded systems analysis and experimental validation*, *Phys. Med. Biol.* **63** (2018) 095003.

[6] S.S. Hsieh, K. Taguchi, S. Leng and C.H. McCollough, *Spatial resolution improvements for photon counting detectors using coincidence counting and frequency weighted reconstruction*, *Med. Phys.* **52** (2025) 2052.

[7] T. Poikela et al., *Timepix3: a 65K channel hybrid pixel readout chip with simultaneous ToA/ToT and sparse readout*, 2014 *JINST* **9** C05013.

[8] T. Michel et al., *Investigating the DQE of the Medipix detector using the multiplicity concept*, in the proceedings of the *2006 IEEE Nuclear Science Symposium Conference Record*, San Diego, CA, U.S.A. (2006), p. 1955–1959 [DOI:10.1109/nssmic.2006.354277].

[9] https://oar.ptb.de/resources/show/10.7795/110.20190315B.



2026 JINST 21 C02024

[10] G. Poludniowski, A. Omar, R. Bujila and P. Andreo, *Technical Note: SpekPy v2.0 — a software toolkit for modeling x-ray tube spectra*, *Med. Phys.* **48** (2021) 3630.

[11] P.W. Nugent, *Measuring the modulation transfer function of an imaging spectrometer with rooflines of opportunity*, *Opt. Eng.* **49** (2010) 103201.

[12] P. Christodoulou et al., *Probability distribution maps of deposited energy with sub-pixel resolution for Timepix3 detectors*, 2024 *JINST* **19** C01026.

2026 JINST 21 C02024